


Synaptic propagation in neuronal networks with finite-support space-dependent couplingRicardo Erazo-Toscano^{✉*} and Remus Osan[†]*Neuroscience Institute, College of Arts and Sciences, Georgia State University, Atlanta, Georgia 30303, USA* (Received 11 February 2019; revised 2 February 2022; accepted 16 December 2022; published 15 March 2023)

Traveling waves of electrical activity are ubiquitous in biological neuronal networks. Traveling waves in the brain are associated with sensory processing, phase coding, and sleep. The neuron and network parameters that determine traveling waves' evolution are the synaptic space constant, synaptic conductance, membrane time constant, and synaptic decay time constant. We used an abstract neuron model in a one-dimensional network to investigate the propagation characteristics of traveling wave activity. We formulate a set of evolution equations based on the network connectivity parameters. Using a combination of numerical and analytical approaches, we show that these traveling waves are stable to a series of perturbations with biological relevance.

DOI: [10.1103/PhysRevE.107.034403](https://doi.org/10.1103/PhysRevE.107.034403)**I. INTRODUCTION**

Waves are physical phenomena observed ubiquitously in nervous systems across taxa. Traveling waves of electrical activity are everywhere in the nervous system. For example, cortical brain waves of activity are found in visual [1–6], olfactory [7,8], auditory [9,10], and motor [11,12] cortices, as well as in the cerebellum [13]. Traveling waves may play roles in working memory [14], sensory processing, phase coding [15,16], and sleep [17]. In the hippocampus, traveling waves of synchronization, such as theta and gamma waves, influence spatial-temporal dynamics [18,19]. Sensorimotor systems rely on traveling waves; for example, in mammals, the spinal cord relays afferent and efferent waves [20]; in fish, the cuttlefish skin pigmentation depends on traveling waves to apply camouflage [21]; in invertebrates, the mollusk olfactory network produces waves when presented with an olfactory stimulus [22]. Understanding the dynamics of traveling waves bridges a gap between observable phenomena and neuroscience theory.

In the present paper we investigate traveling waves in a one-dimensional system where the network is a line of neurons. We restrict the neural dynamics to single-spike integrate-and-fire neuronal network activity propagation [23]. Our model assumes that synaptic connections between neurons are space dependent: The finite support connectivity kernel assumes that synaptic coupling does not decay with distance. One neuron is coupled to all neighboring neurons within one synaptic space constant (synaptic footprint σ). For this system we formulate a system of ordinary differential equations for traveling wave propagation to study the first, second, and potentially higher-order derivatives of firing times as a function of space. The finite support connectivity kernel and the time evolution of spike-dependent synaptic excitation allow the computation of evolution equations in an analytically tractable form. For this work, the evolution equations of

the traveling wave dynamics depend on local dynamics and other parameters with a delayed effect. A key characteristic of our model is that the evolution equations are linear and can be solved analytically.

The finite support connectivity function is mathematically and conceptually more straightforward than other connectivity functions widely used, such as Gaussian [24] or exponential decay [23]. However, constant speed wave dynamics in finite support connectivity kernel are more complicated than waves in networks with exponential decay kernel. Specifically, for the exponential kernel, wave acceleration depends quadratically on instantaneous speed plus delayed parameters, a system with straightforward dynamics [23]. The approach used in the present paper allows us to solve equations for speed and acceleration explicitly and therefore to precisely define how wave speed and acceleration fluctuate as a function of time and space. Overall, the equations of evolution are in excellent agreement with the numerical simulations. The evolution equations predict the traveling wave speed and acceleration based on the network excitability parameters. We further investigate the dynamics of traveling waves with different biologically relevant perturbations; these show that traveling waves are all-or-none events: Waves can only propagate at the speed solution determined by the excitability parameters, or fail to propagate and die off.

II. WAVE EVOLUTION IN the INTEGRATE-AND-FIRE NEURON MODEL

Our theoretical model captures some of the essential dynamics of activity propagation in neuronal networks; the framework has simple assumptions about neuronal excitability and network connectivity. In our simulations, for simplicity, we consider one-dimensional systems where all neurons form a continuous line. We initiate traveling wave activities by applying an external current to a subset of neurons in the network labeled the “shocked region.” Consequently, the neurons in the shocked region spike at the same time (assumed to be $t = 0$). We assume the wave propagates only in the positive direction where we monitor the spiking times

*rjrazo@gmail.com

†osan.remus@gmail.com

of the neurons in the network. As neurons integrate excitatory synaptic inputs, they may reach the firing threshold and spike. Each spike has an excitatory effect on other neurons in the networks, which is usually modeled via a kernel function where nearby neurons receive larger amounts of excitation that vanishes for the ones further apart. Previous research typically examined Gaussian, exponential, and finite support kernels [23–29], leading to the equation in $V(x, t)$ [26],

$$\begin{aligned} \tau_1 \frac{\partial V}{\partial t} &= -V + I_{\text{syn}} \\ &= -V + g_{\text{syn}} \int_D J(|x - y|) \sum_k \alpha(t - t_k(y)) dy, \end{aligned} \quad (1)$$

where

$$\alpha(t) = e^{-t/\tau_2} H(t).$$

Here $t_k(x)$ is the k th spike of the neuron at location x and

$$J(x, y) = J(|x - y|) = \frac{1}{\sigma} H(\sigma - |x - y|),$$

with H the Heaviside function $H(x) = 1$ if $x > 0$ and 0 otherwise. To permit propagation the synaptic integration constant τ_1 needs to be smaller than the decay time of excitation τ_2 , that is, $0 < \tau_1 < \tau_2$, and the synaptic footprint needs to be positive, that is, $\sigma > 0$.

Here we consider traveling waves solutions; therefore, the spiking times of neurons are a monotonic function of their position x within the network. Furthermore, we restrict the analysis to single-spike solutions to facilitate analytical results. Therefore, instead of multiple firing times $t_k(y)$, one only has single spikes across the network, that is, $t(y) = t_1(y)$. Consequently, for a single-spike wave, we can now obtain the integral-form equivalent

$$V(x, t) = \frac{g_{\text{syn}}}{1 - \frac{\tau_1}{\tau_2}} \int_{x-\sigma}^x J(x, y) A(t - t(y)) dy, \quad (2)$$

where

$$A(t) = (e^{-t/\tau_2} - e^{-t/\tau_1}) H(t).$$

The neuronal network model (2) describes the membrane potential V as a function of time- and space-dependent kernels multiplied by the network excitability parameters g_{syn} , σ , τ_1 , and τ_2 (synaptic conductance, synaptic space constant, membrane time constant, and synaptic decay time constant). The neurons are set to spike when $V = V_T$, and this crossing of the threshold results in additional excitation sent by the spiking neuron to other parts of the neural tissue. The parameters of the finite support kernel, x and $x - \sigma$, define the boundaries of the integral. Integrating Eq. (2), the evolution of the wavefront can now be computed as the moment $t(x)$ when the neuron position x spikes, that is, $V(x, t(x)) = V_T$, using the equation

$$\begin{aligned} V(x, t(x)) &= V_T = \frac{g_{\text{syn}}}{1 - \frac{\tau_1}{\tau_2}} [I_2(x, t(x)) - I_1(x, t(x))] \\ &= \frac{g_{\text{syn}}}{1 - \frac{\tau_1}{\tau_2}} \left(e^{-t(x)/\tau_2} \int_{x-\sigma}^x e^{t(y)/\tau_2} dy - e^{-t(x)/\tau_1} \int_{x-\sigma}^x e^{t(y)/\tau_1} dy \right), \end{aligned} \quad (3)$$

where

$$I_i(x, t(x)) = e^{-t(x)/\tau_i} \int_{x-\sigma}^x dy e^{t(y)/\tau_i}, \quad i = 1, 2.$$

Taking the first derivative of Eq. (3), we get the traveling wave speed as a function of integrals I_1 and I_2 :

$$\frac{I_1}{c\tau_1} - \frac{I_2}{c\tau_2} + e^{-[t(x)-t(x-\sigma)]/\tau_1} - e^{-[t(x)-t(x-\sigma)]/\tau_2} = 0. \quad (4)$$

Taking the second derivative of Eq. (3), we obtain

$$\begin{aligned} \frac{dt}{dx} \left(-\frac{1}{\tau_2} + \frac{e^{-[t(x)-t(x-\sigma)]/\tau_2}}{\tau_2} + \frac{1}{\tau_1} - \frac{e^{-[t(x)-t(x-\sigma)]/\tau_1}}{\tau_1} \right) + \left(\frac{dt}{dx} - \frac{dt(x-\sigma)}{dx} \right) \left(\frac{e^{-[t(x)-t(x-\sigma)]/\tau_2}}{\tau_2} - \frac{e^{-[t(x)-t(x-\sigma)]/\tau_1}}{\tau_1} \right) \\ + \frac{d^2t}{dx^2} \left(-\frac{1}{\tau_2} I_2 + \frac{1}{\tau_1} I_1 \right) + \left(\frac{dt}{dx} \right)^2 \left(\frac{1}{\tau_2^2} I_2 - \frac{1}{\tau_1^2} I_1 \right) = 0. \end{aligned} \quad (5)$$

In Eq. (5) we can determine $\frac{d^2t}{dx^2}$ as a function of speed and convert $\frac{d^2t}{dx^2}$ into the instantaneous acceleration. We used the same relationship from Zhang and Osan [23]:

$$a(x) = \frac{d^2x}{dt^2} = -c^3 \frac{d^2t}{dx^2}.$$

The equations of evolution connect the wave speed and acceleration in a similar way to the ones from the exponential kernel [23], but with some major differences that will become apparent later on. We now have a system of two equations where the unknowns are the speed $c(x)$, acceleration $a(x)$, $I_1(x, t(x))$, and $I_2(x, t(x))$. Unfortunately, for these equations we cannot solve the system explicitly, because the network has memory so the wave acceleration at x depends not only on the speed at x , but also on the

speed at $x - \sigma$ and on the difference between the spiking times at these two different spatial locations $\Delta t(x)$. The instantaneous acceleration of the wave propagation then becomes

$$a = \left(\frac{1}{e^{-\Delta t(x)/\tau_2} - e^{-\Delta t(x)/\tau_1}} \right) \left[\frac{V_T \sigma}{g_{\text{syn}} \tau_2} \left(\frac{1}{\tau_2} - \frac{1}{\tau_1} \right) + c \left(\frac{1}{\tau_1} + \frac{1}{\tau_2} \right) (e^{-\Delta t(x)/\tau_1} - e^{-\Delta t(x)/\tau_2}) \right. \\ \left. + c \left(\frac{1}{\tau_1} - \frac{1}{\tau_2} \right) + \left(2c - \frac{c^2}{c(x - \sigma)} \right) \left(\frac{e^{-\Delta t(x)/\tau_2}}{\tau_2} - \frac{e^{-\Delta t(x)/\tau_1}}{\tau_1} \right) \right]. \quad (6)$$

The theoretical wave speed and acceleration are described by Eqs. (6) and (4). The objective of our derivations was to accurately describe the wave propagation based on the excitability parameters and on previous network activity. The system of equations has the following unknown variables: Eq. (4) has $t(x)$ and $t(x - \sigma)$, the spike time of the neuron at the location x and the spike time of neuron at the location $x - \sigma$; Eq. (6) has $c(x)$ and $c(x - \sigma)$, the speed of the wave at the location x and the speed at the location $x - \sigma$.

To confirm our approach, we first conducted simulations to compute the numerical wave speed and acceleration. These estimates are in excellent agreement with theoretical results (Fig. 1). For numerical simulations, neurons in the network are located adjacent to one another and separated by a dis-

cretization constant δ . We performed simulations varying the value of the discretization constant δ . Table I summarizes the percentage of change between numerical simulations with varying magnitudes of δ and the percentage of change between theoretical and numerical speeds.

III. CONSTANT SPEED TRAVELING WAVE

We further explore the equations of evolution to estimate the speed of the traveling wave. We assume two intuitive features: (i) Self-propagating traveling waves reach constant speed asymptotically and (ii) traveling waves that do not self-propagate eventually are extinguished. The acceleration of constant speed waves is zero; therefore, solving Eq. (6) when $a = 0$ yields the consistency equation (7), which describes the neuron membrane potential as a function of traveling wave speed:

$$\sigma V_T \frac{1 - \frac{\tau_1}{\tau_2}}{g_{\text{syn}}} = c(\tau_2 - \tau_1 - \tau_2 e^{-\sigma/c\tau_2} + \tau_1 e^{-\sigma/c\tau_1}). \quad (7)$$

For a traveling wave that arrives from $-\infty$ at a location x and with speed c , one can compute the corresponding voltage. If the voltage is V_T then the solution c is consistent with Eq. (7); otherwise, a traveling wave with speed c cannot exist.

The accuracy of the equations of evolution allows us to estimate the solutions of traveling wave propagation. Figure 2 illustrates that c_{fast} and c_{slow} are located at the intersection between V_T and $V(c)$. Figure 2 also shows that for waves initiated through a shocked region the wave acceleration and speed oscillate while the wave evolves towards the stable state of activity propagation, where $a = 0$ and $c = c_{\text{fast}}$.

Our numerical simulations suggest that traveling waves are all-or-none phenomena, determined by neuronal and network connectivity properties. The parameters g_{syn} (Fig. 3), V_T (Fig. 4), σ (data not shown), τ_1 (data not shown), and τ_2 (data not shown) control traveling wave speed and thus varying any of these parameters beyond a critical value determines wave propagation or failure. Figure 3 shows that as g_{syn} decreases, c_{fast} and c_{slow} become closer in value before disappearing and diverge asymptotically as g_{syn} increases. Figure 4 shows that as V_T increases the wave speed decreases. While Fig. 2 shows that there is a speed at which a wave can induce a maximum V_{max} voltage, Fig. 4 shows that if $V_T > V_{\text{max}}$, the wave fails to propagate. Standard bifurcation analysis is not compatible with the system at hand, because perturbation of the constant speed solutions do not decay back to steady states, as showed by our results in the upcoming sections. In conclusion, our simulations determined that waves are all-or-none events determined by the excitability parameters.

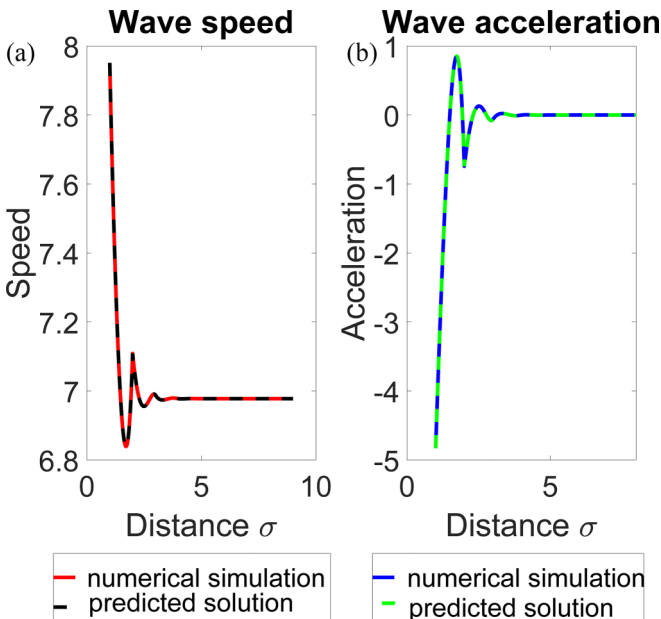


FIG. 1. Comparison of analytical solutions and numerical simulations. The finite support neuronal network of integrate-and-fire neurons with excitatory coupling is at rest; at $t = 0$, the neurons at $x = 0-1$ receive an additional current that drives them over the threshold. All shocked neurons spike synchronously because they receive their input at the same time. The wave evolution shows damped oscillations with an amplitude that decays exponentially. The self-propagating wave settles at the constant speed c_{fast} . (a) Wave speed as a function of space. The red trace is the computer simulation and the black trace is the speed solution from Eq. (4). (b) Traveling wave acceleration as a function of space. The blue trace is the computer simulation and the green trace is the solution from Eq. (6). The parameters are $g_{\text{syn}} = 15$, $\sigma = 1$, $\tau_1 = 1$, $\tau_2 = 2$, $V_T = 1$, and $\delta = 1 \times 10^{-3}$.

TABLE I. Speed and the discretization constant.

δ	Numeric speed	Relative change of numeric speed	Theoretic speed	Relative change of numeric to theoretic speeds
5×10^{-5}	6.984		6.984	0.007%
1×10^{-4}	6.984	0.006%	6.984	0.012%
5×10^{-4}	6.981	0.042%	6.984	0.053%
1×10^{-3}	6.977	0.052%	6.984	0.105%
5×10^{-3}	6.948	0.416%	6.984	0.519%
1×10^{-2}	6.912	0.521%	6.984	1.038%
5×10^{-2}	6.622	4.197%	6.984	5.191%

IV. PERTURBATION-BASED STABILITY ANALYSIS

First, we establish the existence of constant speed traveling waves in neuronal networks of integrate-and-fire neurons with finite support connectivity kernel. According to the consistency equation (7), the threshold V_T constrains the neurons’ membrane potential and traveling wave speed. Figure 2 illustrates that above V_T activity propagation generates additional excitation and below V_T the traveling wave does not generate enough excitation. If the wave travels faster than c_{slow} but slower than c_{fast} , the wave builds a surplus of excitation in the network. In this case, the membrane voltage is higher than

the threshold voltage [Fig. 2(a)]. The surplus of excitation will speed up the activity propagation until the wave speed reaches c_{fast} . If the wave is traveling faster than c_{fast} , the network does not have the resources to sustain activity propagation and the voltage falls lower than the threshold. Then the wave slows down and settles at c_{fast} because, in c_{fast} , the voltage equals V_T . If the wave travels slower than c_{slow} , the voltage is below the threshold and it does not generate enough energy to self-sustain; the wave speed slows down to zero (propagation failure). We ran series of simulations that support this notion; numerically, c_{fast} is stable and c_{slow} is unstable. Next we use a series of approaches to investigate the stability of the constant speed traveling wave. Here the stable speed solution c_{fast} is computed from Eq. (7) as well as determined from numerical simulations and it represents the speed of the constant speed traveling wave.

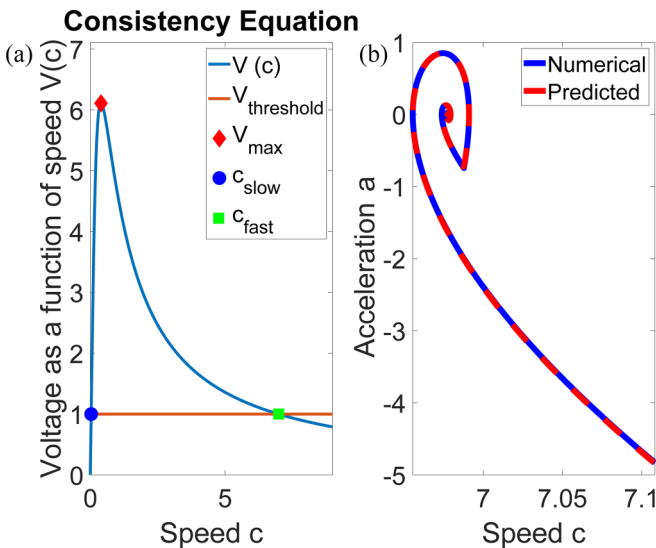


FIG. 2. Stable and unstable fixed points of the wave propagation system. (a) Solutions to the consistency equation as intersections between $V = V(c)$ and the horizontal line at V_T . According to the consistency equation, the neuron membrane potential is a function of traveling wave speed. These numerical solutions allow one to compute both c_{fast} and c_{slow} . Here V_{max} denotes the maximum achievable voltage as a function of the traveling wave speed. If this value is less than V_T no traveling wave can exist. (b) Results from numerical simulations where the wave is initiated through shocking the region $(-\sigma, 0)$. The attractor graph of acceleration as a function of speed indicates that the traveling wave settles into a constant speed solution. The magnitude of the oscillations is consistent with the synaptic footprint space constant σ . The speed c and acceleration a of the traveling wave oscillate while approaching the intersection between $c = c_{fast}$ and $a = 0$. The parameters are $g_{syn} = 15$, $\sigma = 1$, $\tau_1 = 1$, $\tau_2 = 2$, $V_T = 1$, and $\delta = 1 \times 10^{-3}$.

A. Analytical argument for the stability of traveling wave speed

We introduce a small-parameter ϵ perturbation at $t = 0$. This theoretical perturbation consists of imposed initial conditions that force the wave to travel from $x = -\infty$ to $x = 0$

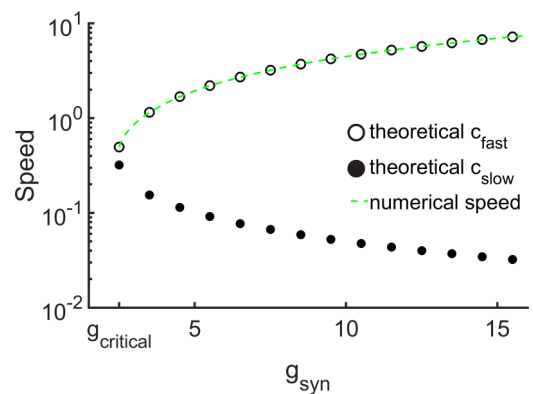


FIG. 3. Traveling wave speed as a function of g_{syn} . This graph represents c_{fast} and c_{slow} as a function of the global excitability parameter, in logarithmic scale. For this set of simulations, we systematically varied g_{syn} and kept all other parameters constant. Our results show there is a critical value g_{crit} where global excitation is so small that traveling wave activities are not sustainable. These curves also illustrate the dependence of the traveling wave dynamics on global excitability: As g_{syn} grows, c_{fast} increases while c_{slow} decreases, both asymptotically. The parameters are $\delta = 1 \times 10^{-3}$, $\sigma = 1$, $\tau_1 = 1$, $\tau_2 = 2$, and $V_T = 1$.

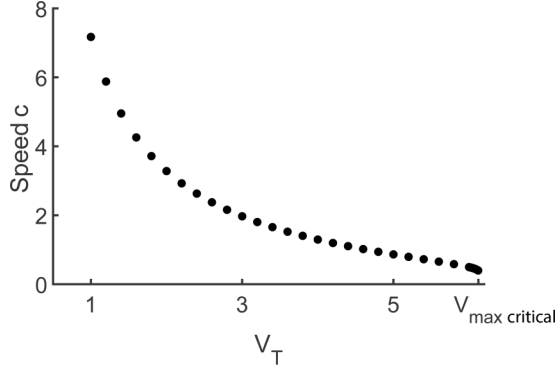


FIG. 4. Traveling wave speed as a function of V_T . For this set of simulations, we systematically varied V_T and kept all other parameters constant. Our results show that as V_T increases, the wave speed decreases. The critical value $V_{\max \text{ critical}}$ is the critical value between activity propagation and failure, determined by the consistency equation (7) (see Fig. 2). Intuitively, when $V_{\max \text{ critical}}$ is found the voltage threshold is greater than the voltage as a function of speed [$V_T \geq V(c)$]. The parameters are $\delta = 1 \times 10^{-3}$, $\sigma = 1$, $g_{\text{syn}} = 15$, $\tau_1 = 1$, $\tau_2 = 2$, $V_T = [1, 6.125]$, and $V_{\max \text{ critical}} = 6.125$.

(practically from $-\sigma$ to 0) at a constant speed faster than c_{fast} . The initial wave speed is defined by

$$c_0 = c_{\text{fast}} + c_1 = c_{\text{fast}} + \epsilon c_{\text{fast}},$$

where $c_1 \ll c_{\text{fast}}$, with a typical value for $\epsilon \approx 0.01$. In this context, the consistency equation becomes

$$c_0(\tau_2 - \tau_1 - \tau_2 e^{-\sigma/c_0 \tau_2} + \tau_1 e^{-\sigma/c_0 \tau_1}) = \sigma \frac{1 - \frac{\tau_1}{\tau_2}}{g_{\text{syn}}} (V_T + \epsilon V_1). \quad (8)$$

For small values of the parameter ϵ , we can look at solutions that are correct in the first order of ϵ by linearizing Eq. (8) to obtain the first-order correction in voltage for $V_0 = V_T + \epsilon V_1$:

$$\epsilon V_1 = \frac{g_{\text{syn}} c_1}{(1 - \frac{\tau_1}{\tau_2})} \left(-\frac{e^{-\sigma/c_{\text{fast}} \tau_2} - e^{-\sigma/c_{\text{fast}} \tau_1}}{c_{\text{fast}}} + \frac{\tau_2 - \tau_1 - (\tau_2 e^{-\sigma/c_{\text{fast}} \tau_2} - \tau_1 e^{-\sigma/c_{\text{fast}} \tau_1})}{\sigma} \right). \quad (9)$$

Intuitively, this means that since the wave is traveling faster than c_{fast} , the neuron at position $x = 0$ will not cross the threshold at $t = 0$, stopping the propagation of the wave temporarily. Therefore, the sign of V_1 is negative and the neuron needs more time to integrate the synaptic currents before potentially crossing the threshold and spiking at a later time, allowing for the wave propagation to restart. The computation of this delay is done next.

In addition to the correction in voltage, the synaptic current also has an order ϵ correction as $I_0 + \epsilon I_1$, with its derivation as follows:

$$I(x, t) = g_{\text{syn}} \int_{x-\sigma}^x e^{-t-t(y)/\tau_2} dy. \quad (10)$$

Since firing times are described by the constant speed traveling wave, it follows that $t(y) = y/c_0$ and

$$I(0^+, t) = I_{\text{syn}} e^{-t/\tau_2} = g_{\text{syn}} \int_{-\sigma}^0 e^{y/c_0 \tau_2} dy e^{-t/\tau_2}, \quad (11)$$

$$I_{\text{syn}} = I_0 + \epsilon I_1 = \frac{g_{\text{syn}}}{\sigma} [(c_{\text{fast}} + c_1) \tau_2 (1 - e^{-\sigma/(c_{\text{fast}} + c_1) \tau_2})]. \quad (12)$$

Finally, we obtain

$$I_0 = \frac{g_{\text{syn}}}{\sigma} [c_{\text{fast}} \tau_2 (1 - e^{-\sigma/c_{\text{fast}} \tau_2})],$$

$$\epsilon I_1 = -c_1 g_{\text{syn}} \left(\frac{e^{-\sigma/c_{\text{fast}} \tau_2}}{c_{\text{fast}}} - \tau_2 \frac{1 - e^{-\sigma/c_{\text{fast}} \tau_2}}{\sigma} \right). \quad (13)$$

The voltage evolution at $x = 0$ follows this explicit formula:

$$V(t) = V_0 e^{-t/\tau_1} + \frac{I_{\text{syn}}}{1 - \frac{\tau_1}{\tau_2}} (e^{-t/\tau_2} - e^{-t/\tau_1}). \quad (14)$$

We can compute the delay in firing for the neuron at $x = 0^+$ by computing the moment when $V(t) = V_T$ in Eq. (14). Again, by focusing only on the first-order Taylor expansion, we obtain the following expression for the delay $\Delta t = t_0$:

$$t_0 = \frac{\epsilon V_1}{\frac{V_T}{\tau_1} - \frac{g_{\text{syn}} \tau_2}{\sigma(1 - \frac{\tau_1}{\tau_2})} c_{\text{fast}} (1 - e^{-\sigma/c_{\text{fast}} \tau_2}) \left(\frac{1}{\tau_1} - \frac{1}{\tau_2} \right)}. \quad (15)$$

To summarize, we investigated how the traveling wave behaved near $x = 0$. We determined that there is a delay once the perturbation is removed. The delay is a function of perturbation speed c_1 and network parameters. In addition to the delay to restart the wave at $x = 0$, namely, t_0 , our methods also allow us to estimate the dynamics of the resuming activity propagation. By using the fact that prior to $x = 0$ we have constant propagation with $t(y) = y/c_0$, we can now use Eqs. (5) and (6) to obtain the restarting speed $c(0^+)$ and acceleration $a(0^+)$ at $x = 0^+$:

$$c(0^+) = -c_{\text{fast}} \frac{e^{-t_0/\tau_2} (1 - e^{-\sigma/c_{\text{fast}} \tau_2}) - e^{-t_0/\tau_1} (1 - e^{-\sigma/c_{\text{fast}} \tau_1})}{e^{-t_0/\tau_2} e^{-\sigma/c_{\text{fast}} \tau_2} - e^{-t_0/\tau_1} e^{-\sigma/c_{\text{fast}} \tau_1}}, \quad (16)$$

$$a(0^+) = \left(\frac{1}{e^{(\sigma + c_{\text{fast}} t_0)/\tau_2} - e^{-(\sigma + c_{\text{fast}} t_0)/\tau_1}} \right) \left[\frac{V_T \sigma}{g_{\text{syn}} \tau_2} \left(\frac{1}{\tau_2} - \frac{1}{\tau_1} \right) + c(0^+) \left(\frac{1}{\tau_1} + \frac{1}{\tau_2} \right) \times (e^{-(\sigma + c_{\text{fast}} t_0)/c_{\text{fast}} \tau_1} - e^{-(\sigma + c_{\text{fast}} t_0)/c_{\text{fast}} \tau_2}) + c(0^+) \left(\frac{1}{\tau_1} - \frac{1}{\tau_2} \right) + \left(2c(0^+) - \frac{c(0^+)^2}{c_{\text{fast}}} \right) \times \left(\frac{e^{-(\sigma + c_{\text{fast}} t_0)/c_{\text{fast}} \tau_2}}{\tau_2} - \frac{e^{-(\sigma + c_{\text{fast}} t_0)/c_{\text{fast}} \tau_1}}{\tau_1} \right) \right]. \quad (17)$$

We now have the initial conditions at $x = 0^+$ to use in conjunction with the system of equations (5) and (6) to determine the wave evolution without resorting to full-network numerical simulations. Figure 5 shows that this approach is in excellent agreement with the numerical simulations from perturbation-imposed initial conditions where the wave propagates from $x = -\infty$ to $x = 0$ at speed greater than c_{fast} . The perturbation is removed at $x = 0$ and the wave further evolves

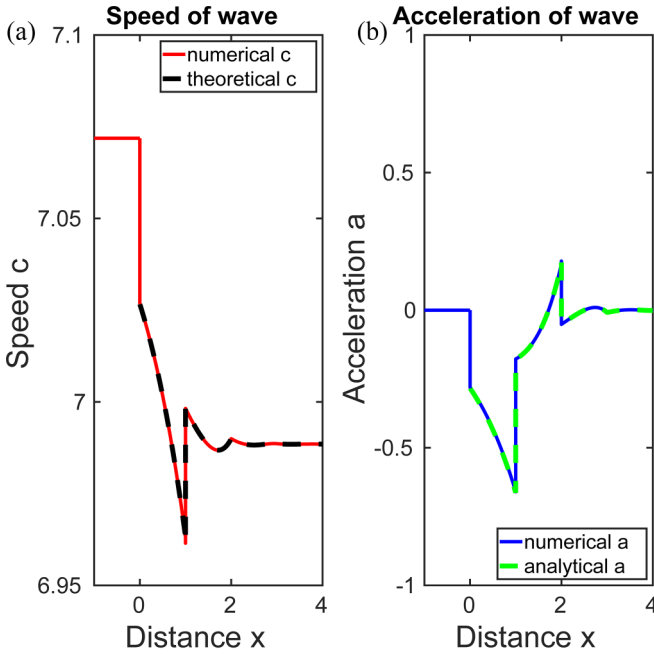


FIG. 5. Faster wave speed perturbation. This graph shows the stability test of the wave speed solution c_{fast} . At $x = 0$, there is no external drive and the wave is free to evolve due to the dynamics defined by network and neuron parameters. Removal of the external drive creates a delay between the spiking time of the last neuron (with external drive) and the first neuron (without external drive). We obtain the following series of estimates: delay from numerical simulation, 8.6253×10^{-4} ; delay from Eq. (15), 8.9347×10^{-4} ; initial speed after the break from simulation, 7.0253; initial speed from Eq. (16), 7.0225; initial acceleration from simulation, -0.2914 ; and initial acceleration from Eq. (17), -0.3095 . $V_1 = -0.928915$. (a) Traveling wave speed as a function of space. The red trace is the computer simulation and the black trace is the result from Eq. (16). (b) Traveling wave acceleration as a function of space. The blue trace is the computer simulation and the green trace is the solution from Eq. (17). Note that acceleration is initially negative (the wave slows down), but then becomes positive because of the oscillations. The parameters are $g_{\text{syn}} = 15$, $\sigma = 1$, $\tau_1 = 1$, $\tau_2 = 2$, $V_T = 1$, $\epsilon = 0.012$, and $\delta = 1 \times 10^{-3}$.

due to the dynamics determined by the neuron and network parameters. Not surprisingly, the traveling wave stops and then restarts with a lower speed than $c_0 = c_{\text{fast}} + c_1$, but at a velocity still higher than c_{fast} .

Together, Figs. 1 and 5 demonstrate that the theoretical framework is in excellent agreement with the numerical simulations. However, as mentioned earlier in the text, the accuracy of the equations depends on the magnitude of ϵ . How accurate are the delay, initial speed, and initial acceleration of the wave from Eqs. (15)–(17) compared to their numerical counterparts? We computed series of simulations with varying magnitudes of ϵ ranging from 0.001 to 0.1, as shown in Fig. 6. We performed linear regression and polynomial regression for these data. The linear and quadratic regressions we performed were both quite accurate, with $R^2 > 0.99$, with marginal improvements by the quadratic method in some cases.

Overall, these results support an argument for the stability of the waves as follows. If the wave travels with a speed c

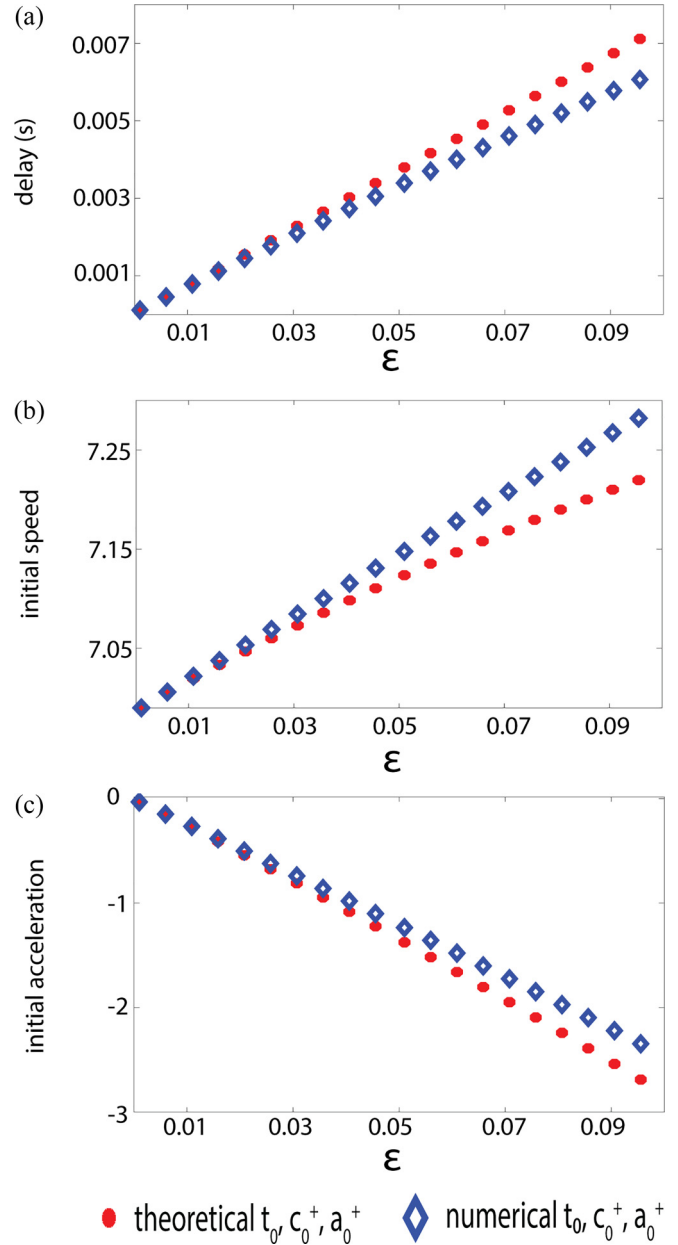


FIG. 6. Accuracy of estimated delays as a function of ϵ . For these graphs, we performed multiple simulations with varying magnitudes for ϵ and saved the delay, speed, and acceleration after the break. Here we summarize the numerical and theoretical values of relevant wave characteristics after removing perturbation: numerical and theoretical t_0 , c_0^+ , and a_0^+ . These numerical and theoretical delays, speeds, and accelerations after perturbation removal show consistent trends dependent on the control parameter ϵ . The range of relative error of t_0 [Eq. (15)] compared to the numerical delay is $[6.2 \times 10^{-6}, 0.0011]$, c_0 [Eq. (16)] relative to the initial speed from simulations is $[2.5 \times 10^{-4}, 0.065]$, and a_0 [Eq. (17)] relative to the numerical acceleration is $[7.2 \times 10^{-4}, 0.35]$. For small values of ϵ , our approximations from Eqs. (15)–(17) are accurate, but as ϵ increases, the system loses accuracy. (a) Delay computed from Eq. (15) and the delay from numerical simulations. (b) Speed computed from Eq. (16) and the speed from numerical simulations. (c) Acceleration computed from Eq. (17) and the acceleration from numerical simulations.

that is faster than c_{fast} until $x = 0$, the tissue at $x > 0$ has a voltage $V < V_T$ at $t = 0$. Consequently, the firing stops for t_0^+ to allow the neuron at $x = 0$ to further increase its voltage and spike at a later time. Due to additional excitation in the system, the waves still restarts with a new speed $c_{\text{fast}} < c_{\text{new}} < c$, that is, the wave still travels faster than needed for stability. As shown by the results in Fig. 6, acceleration a_0^+ is negative for all values of ϵ considered here, effectively acting as a restoring dynamic toward the constant speed traveling wave.

The discontinuity at the spatial boundary of the finite support connectivity kernel complicates solving analytically the evolution of the wave. This is in contrast to the exponential connectivity kernel where the absence of discontinuity within the connectivity kernel (one-way propagation) allows for explicit solutions [23].

While we have examined perturbations with speeds exceeding c_{fast} , the same analysis cannot be performed in a similar way for $c < c_{\text{fast}}$ for the following reasons. The current framework assumes that propagation is monotonic from $-\infty$ to $+\infty$. Waves can accelerate or decelerate but not jump over any region. There is a delay for the fast wave case because the neuron at position $x = 0^+$ needs time to integrate inputs before firing. However, if we implement a slower wave perturbation $-\epsilon$, the neuron at position $x = 0^+$ would fire before the wave arrives and creates a second traveling wavefront. The equations and implementation of nonmonotonic propagating waves with two wavefronts are beyond this paper's scope.

B. Traveling wave stability: Effect of synaptic perturbations such as synaptic inhomogeneity, demyelination, and cell death

We are now set to investigate how perturbations to the microstructure of the neuronal network affect traveling wave propagation. In the synaptic inhomogeneity perturbation, the synaptic coupling parameter g_{syn} is allowed to oscillate sinusoidally as a function of space in a subsection of the network; the result is a sudden increase followed by a sharp decrease in synaptic conductance (Fig. 7) over one period of the sine function. In the demyelination perturbation, the synaptic coupling parameter decreases in a subsection of the network; here the synaptic coupling is relatively weak (Fig. 8). Finally, in the cell death perturbation, the synaptic coupling is completely turned off for a subsection of the network; it emulates the network's activity when the coupled neurons do not spike (Fig. 9). If the subsection is not too large activity can jump over the dead region due to the longer-range connections that can extend over this region. We investigate how the traveling wave speed depends on the synaptic coupling parameter and space constant. Our results are numerical evidence of the stability of the traveling wave solution.

1. Synaptic inhomogeneity perturbation

Synaptic inhomogeneity refers to the media microstructure; it represents periodic variation of strengths of synaptic coupling. We assume g_{syn} is equal throughout the network, except for one synaptic space constant σ , where g_{syn} oscillates sinusoidally with wavelength $\lambda = \sigma$. Here the connections between neurons are stronger, followed by weaker connections than baseline (Fig. 7). These synaptic coupling patterns are common in neuronal networks where neurons from different

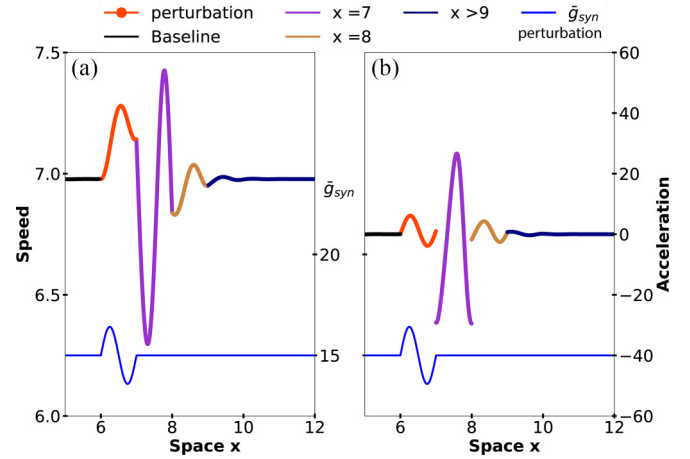


FIG. 7. Wave speed oscillation as a function of both the synaptic coupling and the wave's state. In both panels the wave travels from $x = 0$ to $x = 12$. The blue line at the bottom of the graph represents how $g_{\text{syn}}(x)$ oscillates as a function of space and the sinusoidal perturbation; g_{syn} is constant everywhere else. If $x > 6$ and $x < 7$, $g_{\text{syn}}(x) = g[1 + \epsilon \sin(\frac{2\pi x}{\sigma})]$; otherwise $g_{\text{syn}}(x) = g$. The traveling wave speed fluctuates dramatically while the synaptic inhomogeneity perturbation is present. Because of the effect of the delayed parameters of the finite support kernel, this perturbation produces a peak of traveling wave speed after the perturbation is removed. Interestingly, the magnitude of the second peak is greater than the first peak. (a) The speed of the wave at $x = 7$ affects the speed of the wave at $x = 8$, although the perturbation is totally removed at $x > 7$. The wave speed peaks twice: The increase in local excitability $g_{\text{syn}}(x)$ causes the first peak. The delayed effect of wave speed, i.e., $t(x - \sigma)$ [Eq. (3)] and $c(x - \sigma)$ [Eq. (4)], causes the second peak. This phenomenon exemplifies some of the complicated dynamics of the finite support connectivity kernel compared to the exponential. (b) The traveling wave speed at any given x affects the instantaneous acceleration of the wave of subsequent $x + \sigma$. The instant acceleration oscillates transiently in a sinusoidal fashion while g_{syn} perturbation is present. The parameters are $g = 15$, $\sigma = 1$, $\tau_1 = 1$, $\tau_2 = 2$, $V_T = 1$, $\delta = 1 \times 10^{-3}$, and $\epsilon = 0.0943$.

populations coexist, such as optical preference columns in the visual cortex and the barrel cortex [30]. In our simulations, these synaptic arrangements show interesting transient phenomena while also supporting the stability of the traveling wave speed c_{fast} (Fig. 7).

The traveling wave propagates at a constant speed before the perturbation. The wave speed oscillates at the perturbation location; the speed and acceleration drift away from the stable baseline state. After removing the perturbation, the wave speed continues to oscillate. The oscillations damp while approaching c_{fast} (Fig. 7); while the wave speed approaches c_{fast} , the wave acceleration approaches zero. The wave reaches a constant speed when speed equals c_{fast} and acceleration is 0. Interestingly, the effects of the perturbation are more pronounced during the next two synaptic footprints to the right of the perturbation region.

2. Demyelination perturbation

Synaptic demyelination is a neurodegenerative condition in which neurons lose their myelin sheath. Demyelination

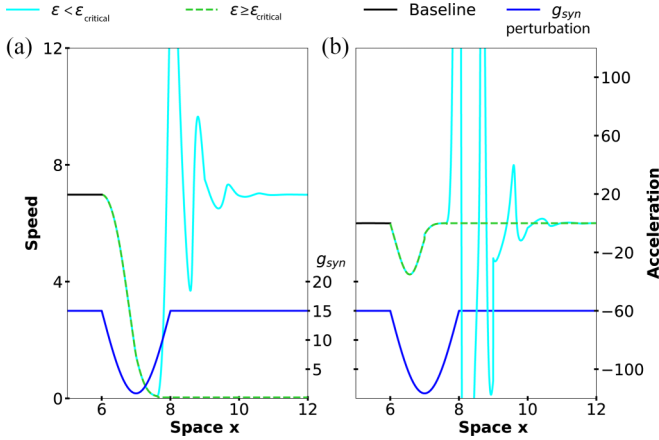


FIG. 8. Neuronal traveling wave phenomena are all-or-none events: One small change in the control parameter separates activity propagation from propagation failure. In both panels the wave travels from $x = 0$ to $x = 12$. The blue line at the bottom of the graph represents how $g_{syn}(x)$ oscillates as a function of space and the demyelination perturbation. At the perturbation, g_{syn} decreases sharply; the g_{syn} decay is determined as follows: If $x > 6$ and $x < 7$, $g_{syn}(x) = g[1 + 10\epsilon \sin(\frac{\pi x}{2\sigma})]$; otherwise $g_{syn}(x) = g$. The cyan and purple wave speeds demonstrate how a small increase in the parameter $\epsilon (\pm 1 \times 10^{-6})$ determines whether the perturbation terminates the wave or the wave continues to propagate after removing the perturbation. The amplitude of the perturbation controls the breaking point of the traveling wave. Here two simulations with the same initial conditions and parameters but with one difference in $\epsilon (\pm 1 \times 10^{-6})$ differ qualitatively. The cyan wave continues to propagate, at wave speed c_{fast} ; the purple wave fails to propagate. The parameters are $g = 15$, $\sigma = 1$, $\tau_1 = 1$, $\tau_2 = 2$, $V_T = 1$, $\epsilon_1 = -0.094289$, $\epsilon_2 = -0.094288$, and $\delta = 1 \times 10^{-3}$.

may be caused by aging [31], Huntington’s disease [32], and ALS [33]. We model the effects of demyelination as a quadratic function; within two synaptic space constants σ , the synaptic coupling between neurons g_{syn} sharply and continuously decreases until reaching a minimum value and returns to the baseline value (Fig. 8). In the demyelination perturbation, the strength of the neuronal connections decreases dramatically in a network subsection. The decrease in g_{syn} synaptic coupling represents the decay of synaptic coupling that is common in demyelinating and neurodegenerative diseases [31–33]. We performed simulations to investigate the traveling wave speed and acceleration with varying magnitudes of perturbations. Consistently with previous sections of the paper, our results strongly suggest that for this class of models, neuronal traveling wave phenomena are all-or-none events (Fig. 8).

The traveling wave propagates at a constant speed before reaching the location of the perturbation. At the perturbation location, g_{syn} decays drastically for one σ ; in the subsequent σ , g_{syn} rapidly recovers the baseline (Fig. 8). The wave travels at a constant speed when it arrives at the perturbation location. Our simulations show a critical value of ϵ (Fig. 8) that separates the waves that recover from those that die off. The waves that recover after removing the perturbation oscillate while approaching c_{fast} ; however, the waves that die off approach c_{slow} (Fig. 8). In conclusion, we demonstrate that extremely

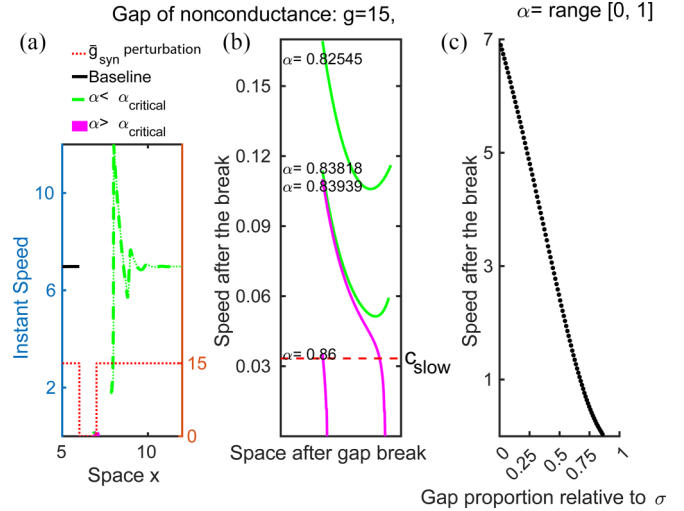


FIG. 9. Dynamics of the traveling wave induced by a nonconducting gap. The simulation consists of a wave traveling at a constant speed c_{fast} . Located at $x = 6$ there is the nonconducting gap of “dead neurons,” which do not spike or synapse. The gap is relative to the synaptic space constant σ and determined by the ratio $\alpha:\sigma$. Waves typically recover from smaller nonconducting gaps; the wave speed oscillates transiently but eventually settles back to a constant speed value, namely, c_{fast} ($\alpha < \alpha_{critical}$, green curves). However, larger perturbations break traveling wave propagation ($\alpha \geq \alpha_{critical}$, magenta curves). The traveling wave’s speed is slower than c_{fast} right where synaptic coupling returns to the baseline; the speed after the break decreases monotonically as α grows and approaches $\alpha_{critical}$. To compute $\alpha_{critical}$, we uniformly sampled 100 points between 0 and 1 and then iterated between 0.8 and 0.86 to find $\alpha_{critical}$ with four-point decimal accuracy. (a) The wave travels at a constant speed arriving at $x = 6$ (black trace). The green and magenta traces show the speed of the wave after the nonconducting gap results from multiple simulations; green curves represent $\alpha < \alpha_{critical}$ and magenta represent $\alpha > \alpha_{critical}$. As the nonconducting gap becomes larger, the wave speed after the break decreases. Larger gaps induce propagation failure. (b) Speed after the gap for the simulations with α near $\alpha_{critical}$. The green and magenta traces show a critical qualitative change in traveling wave evolution as a result of a small parameter change. (c) The speed after the gap is a monotonically decreasing function of the gap size.

small parameter changes could induce dramatic changes in the dynamics of wave evolution; when $\epsilon < \epsilon_{critical}$, the wave recovers, and when $\epsilon > \epsilon_{critical}$, the wave dies off.

3. Cell-death perturbation

We assume synaptic coupling is equal throughout the network, except for a subsection where neurons are not coupled and do not spike. As the wave travels from $-\infty$ toward positive values for x it encounters a nonconducting gap for a finite region, then synaptic coupling returns to baseline values. The gap’s size is determined by the ratio $\alpha:\sigma$, where the value of α ranges from 0 to 1. In the cell-death perturbation, a gap of synaptic nonconductance represents the area of dead neurons. The perturbation methods emulate acute events of neural cell death that may result from cerebral infarction [34] or traumatic brain injury [35,36]; these sorts of insults

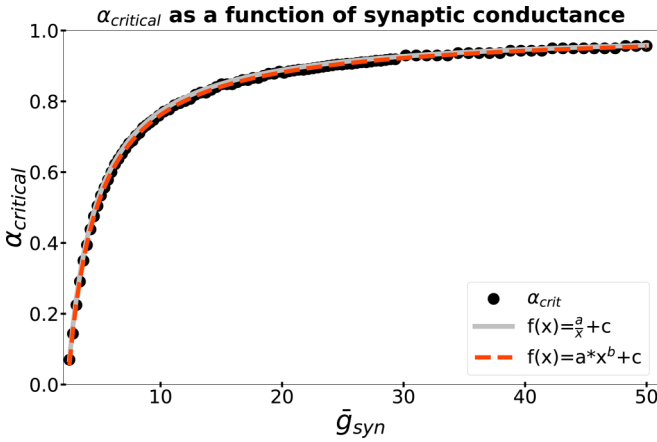


FIG. 10. Smallest gap lengths that induce propagation failure, $\sigma\alpha$. Networks with strong excitatory coupling allow for robust wave propagation. The data above show the critical value of α as a function of network global excitability. The trend demonstrates that with greater excitability, the network's ability to sustain propagating traveling waves is more resilient to nonconducting gaps (areas of dead tissue). Intuitively, this indicates that when overall network excitation is larger, more drastic reduction in the nonconducting gap is needed to produce propagation failure. Curve fit analysis of α_{critical} as a function of g_{syn} demonstrated the power function was a good fit for the curve. Here $f(x) = ax^b + c$. The coefficients (with 95% confidence bounds) are $a = -2.336$ ($-2.357, -2.315$), $b = -0.982$ ($-0.9904, -0.9736$), and $c = 1.005$ ($1.003, 1.007$) [sum of squares error (SSE) equal to 0.00284, $R^2 = 1$, adjusted $R^2 = 1$, root mean square error (RMSE) equal to 0.002918, and $p < 0.1$]. Interestingly, the exponent is so close to -1 that other curves such as $f(x) = \frac{a}{x} + c$ are also a relative good fit (SSE equal to 0.00318, $R^2 = 1$, adjusted $R^2 = 1$, RMSE equal to 0.00317, and $p < 0.01$).

produce neuronal cell death at the location of the accident, while adjacent neurons may survive the insult.

Similar to the other section results, the outcomes from the cell-death perturbation support the idea that constant speed neural waves are all-or-none events and that a small parameter change results in a qualitative difference in wave propagation dynamics (Fig. 9). Computer simulations determine the smallest $\alpha_{\text{critical}}\sigma$ gap that breaks traveling wave propagation (Fig. 10). Here α_{critical} represents the ratio of the synaptic space constant σ in the borderline between traveling wave propagation and failure. Simulations with varying values of g_{syn} demonstrate that α_{critical} is relatively low at low synaptic conductances, but α_{critical} increases rapidly and approaches asymptotically σ as synaptic coupling grows. This indicates that as excitation in the network increases propagation failure is less likely to be triggered, as it requires larger perturbations to suppress the activity in some propagation regions. Figure 10 shows an accurate fit between α_{critical} as a function of g_{syn} and the power function.

V. CONCLUSION AND FUTURE DIRECTIONS

We have presented an extensive analysis of traveling waves in neuronal networks with finite support synaptic coupling. In neuronal networks with exponential or Gaussian connectivity kernels [23], neurons are connected to neighbors up to infinity,

although the connections decay with distance. In contrast, these model networks represent a simplification in network topology by assuming that synapses are strictly space dependent. Connections are only between neighboring neurons within a synaptic footprint σ and zero elsewhere; this simplification is based on the assumption that synaptic coupling is strictly space dependent. However, the finite support kernel introduces discontinuities in the network. The finite support neuronal network proposes a more straightforward mathematical function and biological structure compared to other connectivity functions, such as Gaussian or exponential. Despite the inherent simplicity in the finite support function, the mathematical model is complicated and has no analytical solutions. However, we managed to describe wave propagation as a set of evolution equations that predict wave dynamics without the need to run the entire computer simulation [Eqs. (4), (6), (16), and (17)].

In order to investigate the stability of the wave, we presented a number of perturbations. First was a traveling wave going from $-\infty$ to 0 at a constant speed $c_0 = c_{\text{fast}} + \epsilon c_{\text{fast}}$. Simulations and analytical studies showed there is a delay to spike once the perturbation is removed. We computed the delay, speed, and acceleration after the break in Eqs. (15), (16), and (17), respectively. We then presented perturbations relevant to a biological context, resembling the effects of demyelinating disorders and cell death. Demyelinating disorders were presented as continuous perturbations (Fig. 8) in the topology of the parameter g_{syn} in a subsection of the network. These results were consistent with the notion that synaptic coupling facilitates traveling wave propagation: In the cases in which the introduced perturbation increased coupling, the wave accelerated; in the cases in which the perturbation decreased coupling, the wave decelerated (Fig. 7). If the wave decelerates slower than c_{slow} , propagation fails to continue (Figs. 8 and 9). The last perturbation we presented was a nonconducting gap, which resembles a small section of dead tissue (Fig. 9). The gap was defined as $\alpha\sigma$ and represented the ratio $\alpha:\sigma$. For any given g_{syn} there is a corresponding critical value $\epsilon_{\text{critical}}$ between activity propagation and failure (Fig. 10). The demyelination and dead tissue perturbations (Figs. 8 and 9, respectively) show remarkable stability of the system because despite how much the perturbation decelerated the wave, all the waves that continued to propagate evolved back to the steady state c_{fast} .

Altogether, the present work has demonstrated that waves respond robustly in neuronal networks with finite support coupling and that network parameters influence traveling wave propagating speed. Waves in neuroscience are ubiquitous and unraveling population dynamics can inform us of underlying mechanisms that give rise to neuronal function and dysfunction. For example, the inhomogeneity perturbation (Fig. 7) shows how the speed of neuronal activity can fluctuate if there is a subsection of tightly coupled neurons. On the other hand, the demyelination perturbation suggests that because waves are all-or-none phenomena, they represent a resilient mechanism for neuronal communication. Demyelination is common in myelination diseases, such as Huntington's disease and multiple sclerosis. In this framework, it is intuitive to understand why many symptoms are not expressed until demyelination reaches a critical point, at which neuronal

function falls apart. Likewise, the nonconducting gap of dead tissue (Fig. 9) may be an example of postinfarction neuronal tissue. This hypothesis could explain the impairment of neuronal functions in the context of the local characteristics and the topology of the network where the cerebral infarction took place.

The exponential connectivity kernel imposes the longest-reaching connections e^{-x} [23]. The finite support kernel imposes the shortest-ranging connections. Future studies could focus on the Gaussian kernel, which imposes midrange connections e^{-x^2} . However, the derivation of the evolution equations becomes more complicated for the Gaussian kernel inside the integral. For example, the first derivative of the Gaussian kernel e^{-x^2} results in some integral terms that did not exist before, such as xe^{-x^2} . Furthermore, for additional

derivatives, while some terms revert to existing factors, others correspond to higher-order polynomials, such as $x^2e^{-x^2}$ for the second-order derivative. As a result, it is impossible to fully solve this infinite system of equations, although it could be possible to attempt to solve a finite system of equations that approximate the full one.

ACKNOWLEDGMENT

We acknowledge the support of NIH Grant No. 1R21NS111355 to Gennady Cymbalyuk and Ronald Calabrese, an industry grant from Decanex, Inc. Toronto, Canada to Remus Osan, and a Georgia State University Neuroscience Institute Brains and Behavior Fellowship granted to Ricardo Erazo-Toscano.

-
- [1] T. K. Sato, I. Nauhaus, and M. Carandini, Traveling waves in visual cortex, *Neuron* **75**, 218 (2012).
 - [2] T. Wanger, K. Takagaki, M. T. Lippert, J. Goldschmidt, and F. W. Ohl, Wave propagation of cortical population activity under urethane anesthesia is state dependent, *BMC Neurosci.* **14**, 78 (2013).
 - [3] J. B. Ackman and M. C. Crair, Role of emergent neural activity in visual map development, *Curr. Opin. Neurobiol.* **24**, 166 (2014).
 - [4] J. B. Ackman, T. J. Burbridge, and M. C. Crair, Retinal waves coordinate patterned activity throughout the developing visual system, *Nature (London)* **490**, 219 (2012).
 - [5] T. P. Zanos, P. J. Mineault, K. T. Nasiatou, D. Guitton, and C. C. Pack, A sensorimotor role for traveling waves in primate visual cortex, *Neuron* **85**, 615 (2015).
 - [6] I. Nauhaus, L. Busse, D. L. Ringach, and M. Carandini, Robustness of traveling waves in ongoing activity of visual cortex, *J. Neurosci.* **32**, 3088 (2012).
 - [7] A. Compte, M. V. Sanchez-Vives, D. A. McCormick, and X.-J. Wang, Cellular and network mechanisms of slow oscillatory activity (<1 Hz) and wave propagations in a cortical network model, *J. Neurophysiol.* **89**, 2707 (2003).
 - [8] M. Murakami, H. Kashiwadani, Y. Kirino, and K. Mori, State-dependent sensory gating in olfactory cortex, *Neuron* **46**, 285 (2005).
 - [9] A. Reimer, P. Hubka, A. K. Engel, and A. Kral, Fast propagating waves within the rodent auditory cortex, *Cereb. Cortex* **21**, 166 (2011).
 - [10] M. Chrostowski, L. Yang, H. R. Wilson, I. C. Bruce, and S. Becker, Can homeostatic plasticity in deafferented primary auditory cortex lead to travelling waves of excitation? *J. Comput. Neurosci.* **30**, 279 (2011).
 - [11] D. R. Belov, P. A. Stepanova, and S. F. Kolodyazhnyi, Traveling waves in the human EEG during voluntary hand movements, *Neurosci. Behav. Physiol.* **45**, 1043 (2015).
 - [12] D. Rubino, K. A. Robbins, and N. G. Hatsopoulos, Propagating waves mediate information transfer in the motor cortex, *Nat. Neurosci.* **9**, 1549 (2006).
 - [13] S. Dipierro and E. Valdinoci, A simple mathematical model inspired by the Purkinje cells: From delayed travelling waves to fractional diffusion, *Bull. Math. Biol.* **80**, 1849 (2018).
 - [14] D. B. Poll and Z. P. Kilpatrick, Velocity integration in a multilayer neural field model of spatial working memory, *SIAM J. Appl. Dyn. Syst.* **16**, 1197 (2017).
 - [15] K. Takahashi, M. Saleh, R. D. Penn, and N. Hatsopoulos, Propagating waves in human motor cortex, *Front. Hum. Neurosci.* **5**, 40 (2011).
 - [16] A. Bahramsharif, M. A. J. van Gerven, E. J. Aarnoutse, M. R. Mercier, T. H. Schwartz, J. J. Foxe, N. F. Ramsey, and O. Jensen, Propagating neocortical gamma bursts are coordinated by traveling alpha waves, *J. Neurosci.* **33**, 18849 (2013).
 - [17] M. Massimini, R. Huber, F. Ferrarelli, S. Hill, and G. Tononi, The sleep slow oscillation as a traveling wave, *J. Neurosci.* **24**, 6862 (2004).
 - [18] E. V. Lubenov and A. G. Siapas, Hippocampal theta oscillations are travelling waves, *Nature (London)* **459**, 534 (2009).
 - [19] H. Zhang and J. Jacobs, Traveling theta waves in the human hippocampus, *J. Neurosci.* **35**, 12477 (2015).
 - [20] C. A. Cuellar, J. A. Tapia, V. Juárez, J. Quevedo, P. Linares, L. Martínez, and E. Manjarrez, Propagation of sinusoidal electrical waves along the spinal cord during a fictive motor task, *J. Neurosci.* **29**, 798 (2009).
 - [21] A. Laan, T. Gutnick, M. J. Kuba, and G. Laurent, Behavioral analysis of cuttlefish traveling waves and its implications for neural control, *Curr. Biol.* **24**, 1737 (2014).
 - [22] D. Kleinfeld, K. R. Delaney, M. S. Fee, J. A. Flores, D. W. Tank, and A. Gelperin, Dynamics of propagating waves in the olfactory network of a terrestrial mollusk: An electrical and optical study, *J. Neurophysiol.* **72**, 1402 (1994).
 - [23] J. Zhang and R. Osan, Analytically tractable studies of traveling waves of activity in integrate-and-fire neural networks, *Phys. Rev. E* **93**, 052228 (2016).
 - [24] R. Osan and B. Ermentrout, The evolution of synaptically generated waves in one- and two-dimensional domains, *Physica D* **163**, 217 (2002).
 - [25] R. Osan, R. Curtu, J. Rubin, and B. Ermentrout, Multiple-spike waves in a one-dimensional integrate-and-fire neural network, *J. Math. Biol.* **48**, 243 (2004).
 - [26] R. Osan, J. Rubin, R. Curtu, and B. Ermentrout, Traveling waves in a one-dimensional integrate-and-fire neural network with finite support connectivity, *Neurocomputing* **52–54**, 869 (2003).

- [27] R. Osan and B. Ermentrout, Two dimensional synaptically generated traveling waves in a theta-neuron neural network, *Neurocomputing* **38–40**, 789 (2001).
- [28] B. Ermentrout, The analysis of synaptically generated traveling waves, *J. Comput. Neurosci.* **5**, 191 (1998).
- [29] B. Ermentrout, J. Rubin, and R. Osan, Regular traveling waves in a one-dimensional network of theta neurons, *SIAM J. Appl. Math.* **62**, 1197 (2002).
- [30] *Principles of Neural Science*, 4th ed., edited by E. R. Kandel, J. H. Schwartz, and T. M. Jessell (McGraw-Hill, New York, 2000).
- [31] A. M. Adinolfi, J. Yamuy, F. R. Morales, and M. H. Chase, Segmental demyelination in peripheral nerves of old cats, *Neurobiol. Aging* **12**, 175 (1991).
- [32] O. Phillips, C. Sanchez-Castaneda, F. Elifani, V. Maglione, A. Di Pardo, C. Caltagirone, F. Squitieri, U. Sabatini, and M. Di Paola, Tractography of the corpus callosum in Huntington's disease, *PLoS One* **8**, e73280 (2013).
- [33] S. H. Kang, Y. Li, M. Fukaya, I. Lorenzini, D. W. Cleveland, L. W. Ostrow, J. D. Rothstein, and D. E. Bergles, Degeneration and impaired regeneration of gray matter oligodendrocytes in amyotrophic lateral sclerosis, *Nat. Neurosci.* **16**, 571 (2013).
- [34] I. Ferrer and A. M. Planas, Signaling of cell death and cell survival following focal cerebral ischemia: Life and death struggle in the penumbra, *J. Neuropathol. Exp. Neurol.* **62**, 329 (2003).
- [35] R. Raghupathi, Cell death mechanisms following traumatic brain injury, *Brain Pathol.* **14**, 215 (2004).
- [36] A. Rink, K. M. Fung, J. Q. Trojanowski, V. Lee, E. Neugebauer, and T. K. McIntosh, Evidence of apoptotic cell death after experimental traumatic brain injury in the rat, *Am. J. Pathol.* **147**, 1575 (1995).